Analysis of transitional polymeric flows and elastic instabilities

By Y. Dubief†, V. E. Terrapon‡ AND J. Soria¶‖

The dynamics of turbulence generated and controlled by polymer additives is investigated from the perspective of the coupling between polymer dynamics and flow structures. Direct numerical simulations of channel flow with Reynolds numbers ranging from 1,000 to 10,000 (based on the bulk and the channel height) are used to study the formation and dynamics of elastic instabilities and their effects on the flow. The resulting mechanism of interactions between polymer dynamics and the flow helps resolve a long-standing controversy in the understanding of polymer drag reduction and explains the phenomenon of early turbulence, or onset of turbulence at lower Reynolds numbers than for Newtonian flows, previously observed in polymeric flows.

1. Introduction

Polymer additives are known for producing upward of 80% of drag reduction in turbulent wall-bounded flows through a strong alteration and reduction of the turbulent activity (White & Mungal 2008). The changes in flow dynamics induced by polymers do not lead to flow relaminarization but, at most, to a universal asymptotic state called maximum drag reduction (MDR). The early quantitative description of MDR (Virk *et al.* 1970) was semi-empirical, yielding a correlation for the friction factor and the Virk log-law mean velocity profile. Recently, Procaccia *et al.* (2008) proposed a theory that derives, in the limit of infinite Reynolds number, an asymptotic log-law for the mean velocity profile remarkably close to Virk's. However, the existence of a logarithmic region in the mean velocity profile of MDR is not verified by currently available experiments and simulations (White *et al.* 2012).

The theory of MDR derived by Procaccia *et al.* describes the action of polymers as an eddy viscosity linearly increasing with increasing distance to the wall. Most noticeably, the theory assumes that "In contradistinction to the picture offered by de Gennes, simulations (performed by the authors) indicate that the energy never goes back from the polymers to the flow; the only thing that polymers can do is to increase the dissipation" (quote from Procaccia *et al.* 2008). This statement is at odds with the mechanism of polymer drag reduction and two other unique properties of polymer solutions, elastic turbulence and elasto-inertial turbulence. These three phenomena support De Gennes (1990)'s picture that drag reduction derives from two-way energy transfers between turbulent kinetic energy of the flow and elastic energy of polymers at small scales, resulting into the overall modification of the turbulence energy cascade at high Reynolds numbers.

The drag reducing mechanism is caused by an increase of the (extensional) viscosity in

† School of Engineering, University of Vermont, USA
‡ Aerospace and Mechanical Engineering Department, University of Liège, Belgium
¶ Department of Mechanical and Aerospace Engineering, Monash University, Australia
‖ Department of Aeronautical Engineering, King Abdulaziz University, Jeddah, Kingdom of Saudi Arabia

extensional upwash and downwash flows generated by quasi-streamwise vortices (Dubief *et al.* 2004; Terrapon *et al.* 2004), thereby creating a negative torque on these near-wall vortices (Kim *et al.* 2007). Dubief *et al.* (2004) demonstrated that polymers re-inject part of the energy accumulated in high-speed streaks, regions of locally high-speed flow in the near-wall region elongated in the direction of the flow. In inertia-less flows with curved streamlines, Groisman & Steinberg (2000) demonstrated the existence of strong non-linear mixing supported by elastic turbulence, a state of saturated dynamical interactions between stretched polymer molecules and the base flow that causes the stretching.

The present paper focuses on the last evidence of energy transfer from polymers to flow, the recently discovered elasto-inertial turbulence, hereafter referred to as EIT (Samanta *et al.* 2012). EIT is a new state of small-scale turbulence driven by the interaction between elastic instabilities and the flow's inertia that has been observed over a wide range of Reynolds numbers, from subcritical to high Reynolds numbers. EIT exists by either creating its own extensional flow patterns, as we will demonstrate here in subcritical channel flows, or by exploiting extensional flow topologies, as we shall observe in the wake of hairpin vortex at a higher Reynolds numbers. EIT offers an alternative description of MDR that has the merit of explaining not only the absence of log-law in finite-Reynolds numbers MDR flows but also the phenomenon of early turbulence (Hoyt 1977), which describes the onset of turbulence in the presence of diluted polymer additives at Reynolds numbers significantly smaller than in the absence of polymers.

2. Method

Channel flow simulations are performed in a cartesian domain, where x, y and z are the streamwise, wall-normal and spanwise directions, respectively. For a polymer solution, the flow transport equations are the conservation of mass, $\boldsymbol{\nabla}\cdot\mathbf{u}=0$, where $\mathbf{u}$ is the velocity vector, and transport of momentum:

$$\partial_t\mathbf{u}+(\mathbf{u}\cdot\boldsymbol{\nabla})\mathbf{u}=-\boldsymbol{\nabla}p+\frac{\beta}{Re}\nabla^2\mathbf{u}+\frac{1-\beta}{Re}\boldsymbol{\nabla}\cdot\mathbf{T}\,. \tag{2.1}$$

The Reynolds number is based on the bulk velocity U_b and the full channel height $H=2h$, $Re=U_bH/\nu$. The parameter β is the ratio of solvent viscosity to the zero-shear viscosity of the polymer solution and affects both the viscous stress and polymer stress terms in Eq. (2.1). The polymer stress tensor $\mathbf{T}$ is computed using the FENE-P (Finite Elastic Non-linear Extensibility-Peterlin) model (Bird *et al.* 1987):

$$\mathbf{T}=\frac{1}{Wi}\left(\frac{\mathbf{C}}{1-\mathrm{tr}(\mathbf{C})/L^2}-\mathbf{I}\right)\,, \tag{2.2}$$

where the tensor $\mathbf{C}$ is the local conformation tensor of the polymer solution and $\mathbf{I}$ is the unit tensor. The properties of the polymer solution are β, the maximum polymer extension L, and the Weissenberg number Wi based on the solution relaxation time λ and the flow time scale relevant to the dynamics of interest. Here Wi is based on the wall shear-rate $\dot\gamma$ of the initial laminar flow at each Re, hence $Wi=\lambda\dot\gamma$. The FENE-P model assumes that polymers may be represented by a pair of beads connected by a nonlinear spring defined by the end-to-end vector $\mathbf{q}$. The conformation tensor is the phase-average of the tensorial product of the end-to-end vector $\mathbf{q}$ with itself, $\mathbf{C}=\langle\mathbf{q}\otimes\mathbf{q}\rangle$, whose transport equation is

$$\partial_t\mathbf{C}+(\mathbf{u}\cdot\boldsymbol{\nabla})\mathbf{C}=\mathbf{C}(\boldsymbol{\nabla}\mathbf{u})+(\boldsymbol{\nabla}\mathbf{u})^{\mathrm{T}}\mathbf{C}-\mathbf{T}\,. \tag{2.3}$$

On the right-hand side of Eq. (2.3), the first two terms are responsible for the stretching of polymers by hydrodynamic forces, whereas the third term models the internal energy that tends to bring stretched polymers to their least energetic state (coiled).

Eqs. (2.1-2.3) are solved using finite differences on a staggered grid and a semi-implicit time advancement scheme described elsewhere (Dubief *et al.* 2005). A series of simulations was carried out for Reynolds numbers ranging from 1000 to 6000. A thorough resolution study led us to choose a domain size of $10H \times H \times 5H$ with $256 \times 151 \times 256$ computational nodes. All results discussed here have been verified on domains with a factor 2 in horizontal dimensions and resolution in each directions. The CFL number was set to 0.15 to guarantee the boundedness of $\mathbf{C}$.

The protocol for our simulations was designed to mimic the perturbed experimental setup of Samanta *et al.* (2012) within the limitation inherent to the DNS boundary conditions. For any flow, Newtonian or polymeric, the initial flow and polymer fields are first equilibrated to the laminar state corresponding to the desired Re. A perturbation is then introduced over a short duration, in the form of blowing and suction velocity on both walls, over which white noise of prescribed intensity is introduced. The velocity pattern is periodic in x and z:

$$v_w(x,z,t) = \mathcal{H}(t)\left[A\sin\left(\frac{8\pi}{L_x}x\right)\sin\left(\frac{8\pi}{L_z}z\right)+\varepsilon(t)\right], \tag{2.4}$$

where A is the amplitude, L_x and L_z are the horizontal domain dimensions, and $\varepsilon(t)$ is the random noise. The total duration of the perturbation is $0.5h/U_b$, of which the first and last 10% correspond to a gradual increase/decrease through a smooth step function $\mathcal{H}(t)$. Choosing $A = 0.09U_b$ and the RMS of ε at $0.005U_b$ causes the Newtonian flow to transition at $Re = 6000$.

All polymeric simulations are performed with $L = 200$ and $\beta = 0.9$. Two Weissenberg numbers are considered, $Wi = 100$ and 700. The former is consistent with previous simulations of MDR (Dubief *et al.* 2004; Li *et al.* 2006; White *et al.* 2012). Procaccia *et al.* (2008)'s theory, based on infinite Re and Wi, motivates the second, as an exploration of the effects of very large elasticity, or Wi, on the flow.

3. Some statistical properties of EIT

Figure 1 summarizes the main statistical properties of our simulations. Figure 1(a) shows the evolution of the friction factor as a function of the Reynolds number from $Re = 1000$ to 6000. In excellent agreement with experiments (Samanta *et al.* 2012), the friction factor of polymeric flows departs from the laminar asymptote, with a slight drag increase, to transition smoothly to the MDR asymptote, where drag is reduced compared to turbulent flow. The effects of increasing elasticity is only noticeable at higher Reynolds numbers with more pronounced drag reduction.

Figure 1(b) compares the mean velocity profiles U normalized by the bulk velocity U_b for two Reynolds numbers, $Re = 1000$ and 6000, representative of the two domains $Re < Re_c$ and $Re > Re_c$, where Re_c is defined as the intersection of the laminar and MDR asymptotes, $Re_c = 1791$. In the first domain, the mean velocity profile departs only slightly from the Newtonian Poiseuille solution for laminar flow. In the second domain, the mean velocity profile is significantly affected, and, as expected, different from Newtonian turbulence at the same Re. The polymeric flow at $Re = 1000$ produces modest, yet non-zero, turbulent kinetic energy (TKE), peaking at about a quarter of the

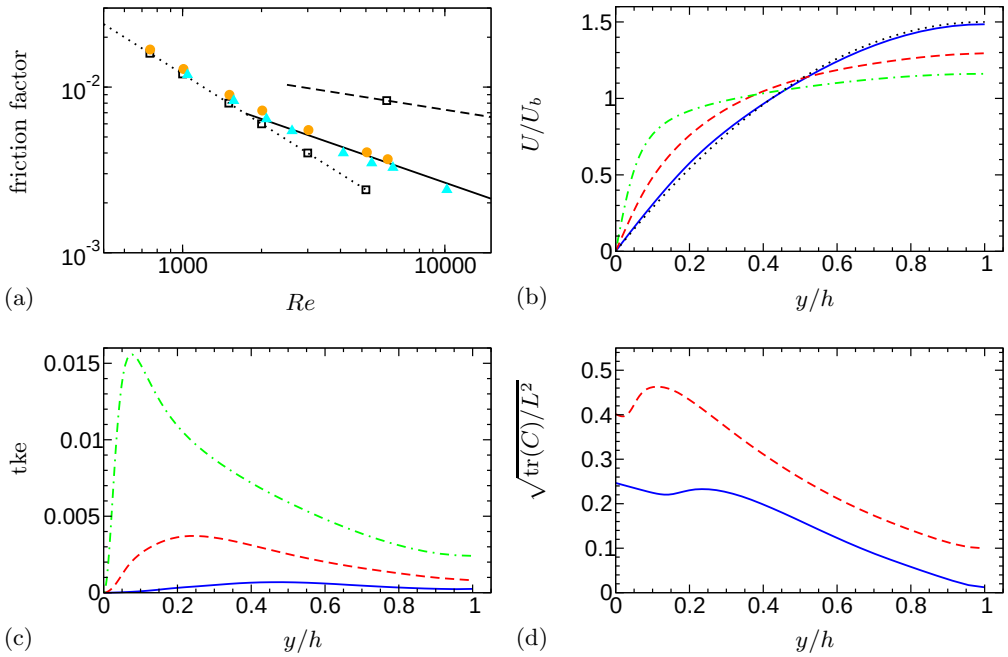

FIGURE 1. (a) Shows the friction factor as a function of Reynolds number for two Weissenberg numbers $Wi = 100$ (●), $Wi = 700$ (▲) with $L = 200$ and $\beta = 0.9$. Lines indicate correlations for Laminar (····· , $f = 12/Re$) and turbulent (– – – – , $f = 0.073Re^{-1/4}$) Newtonian channel flow and for MDR (——— , $f = 0.42Re^{-0.55}$); Newtonian solutions are also included (□). (b) and (c) Display the mean velocity profiles and profiles of turbulent kinetic energy, respectively, for polymeric simulations with $Wi = 100$ at $Re = 1000$ (——— , compared to the Poiseuille laminar solution ·····) and $Re = 6000$ (– – – –), and for fully turbulent Newtonian flow at $Re = 6000$ (— · —). (d) Shows the profile of polymer extension corresponding to the polymeric flows used in (b) and (c). (Color online.)

channel height from the wall. At $Re = 6000$, TKE is significantly reduced compared to Newtonian turbulence.

Lastly, Figure 1 shows the profiles of polymer stretch, defined by $\sqrt{\mathrm{tr}(C)/L^2}$, for the two Reynolds numbers of interest. The mean polymer stretch is well below 50% of full extension, indicating that the mechanism at play is not induced by coil-stretch transition, at least from the perspective of time-averaged transport equations. In a purely laminar flow, the solution for $\sqrt{\mathrm{tr}(C)/L^2}$ decreases monotonically. The emergence of a local maximum away from the wall at our lowest Reynolds number suggests a departure of the flow from pure shear flow. Indeed, the local maximum of polymer at $Re = 6000$ arises from the interactions between polymers and turbulent structures in the buffer region, in particular vortices, which produce local extensional flows with dramatic effects on the polymer dynamics (Terrapon *et al.* 2004). The possible existence of extensional flow topology at $Re = 1000$ is the motivation for our topological study.

4. Topology of EIT

The flow topology is a critical component of the dynamics of polymers (Terrapon *et al.* 2004), since it governs the stretching terms in the transport equation of the conformation

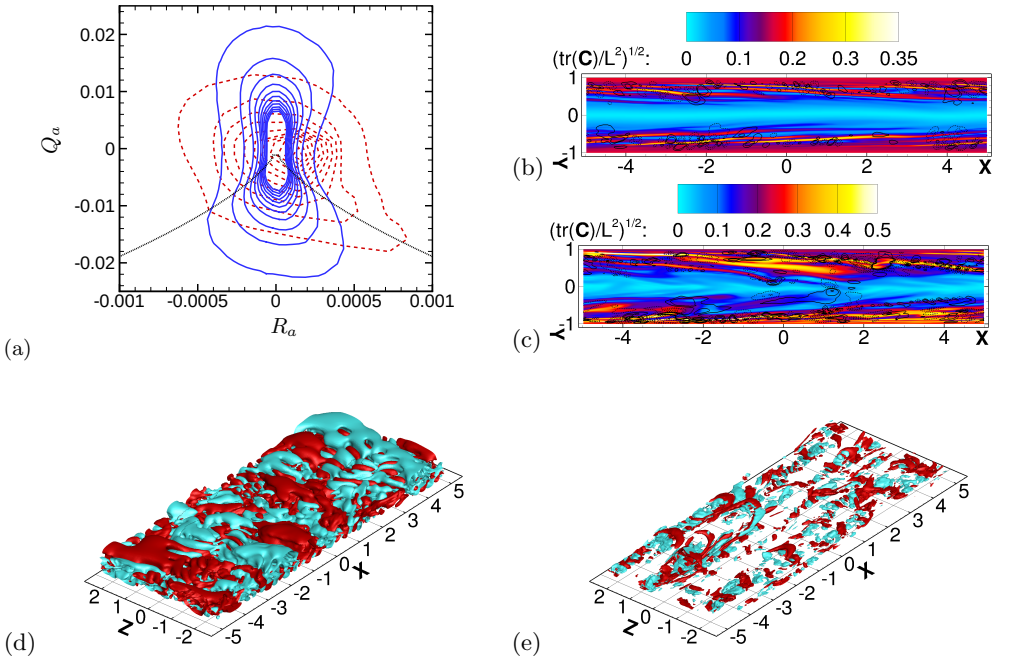

FIGURE 2. (a) Shows the joint probability density functions of flow topology in the (Q_a, R_a) phase plot for polymeric flows at $Re = 1000$ (———) and 6000 for $Wi = 100$ (- - - -). Line ····· describes $D = 27/4R_a^2 + Q_a^3 = 0$, the vertical bounds of the four quadrants of flow topology. Instantaneous contours of polymer extension in an $x - y$ plane showing streamwise sheet-like regions for $Re = 1000$ (b) and $Re = 6000$ (c); the continuous and dashed lines superimposed to the contours of polymer stretch represent isosurfaces of Q_a. Instantaneous isosurfaces of the second invariant of the velocity gradient tensor for $Q_a = \pm 0.025$ at $Re = 1000$ (d) and $Q_a = \pm 0.25$ at $Re = 6000$ (e). Red: positive Q_a; cyan: negative Q_a. (Color online.)

tensor, Eq. (2.3), through the velocity gradient tensor $\boldsymbol{\nabla}\mathbf{u} = \partial_j u_i$. We therefore apply the classical reduction of the flow into a joint probability density function (jpdf) of the second $Q_a = -\partial_j u_i \partial_i u_j/2$ and third $R_a = -\partial_j u_i \partial_k u_j \partial_j u_k/3$ invariants of $\boldsymbol{\nabla}\mathbf{u}$ (Soria *et al.* 1994; Ooi *et al.* 1999). Based on the sign of the discriminant $D = 27/4R_a^2 + Q_a^3$, quadrants I ($R_a > 0, D > 0$) and II ($R_a < 0, D > 0$) of Figure 2(a) define spiraling flows under compression and extension, respectively, and III ($R_a < 0, D < 0$) and IV ($R_a > 0, D < 0$) biaxial compressional and extensional flows, respectively. At $Re = 6000$, the jpdf contours exhibit an inverted teardrop shape common to many turbulent flows, in particular of Newtonian turbulent channel flow. The topology distribution for the lower Reynolds number flow is significantly different with a quasi-symmetry around both $R_a = 0$ and $Q_a = 0$ and the confirmation of the existence of biaxial extensional events ($D < 0$). Local extensional flows are captured in contours of polymer stretch (Figure 2b) in the form of thin sheets of locally high polymer stretch, tilted upwards and elongated in the flow direction. At $Re = 6000$ (Figure 2c), the structure of the polymer stretch field is similar. In Figures 2(b-c), superimposed to the contours of polymer stretch are the contours of positive and negative Q_a which reveal the existence of trains of circular regions of alternating Q_a-sign associated to sheets of large polymer stretch. Figures 2(d-e) show the 3D structure of Q_a with positive and negative isosurfaces of Q_a for $Re = 1000$

and 6000, respectively. At the lower Reynolds number, the structure of the Q_a field is predominantly spanwise with trains of cylindrical structures of various scales. At the higher Reynolds numbers, a few hairpin-like vortices can be observed as well as trains of spanwise cylindrical structures of alternating signs. Such trains have also been observed in the wake of heads of hairpin vortices at even higher Reynolds numbers (Dubief *et al.* 2010).

The dynamic of EIT is therefore consistent across the two regimes shown in Figure 1(a) ($Re < Re_c$ and $Re > Re_c$), and is best described by (i) taking the divergence of Eq. (2.1), which yields the Poisson equation for pressure in a viscoelastic flow:

$$\nabla^2 p = 2Q_a - \frac{1-\beta}{Re}\boldsymbol{\nabla}\cdot(\boldsymbol{\nabla}\cdot\mathbf{T}), \tag{4.1}$$

and (ii) considering the hyperbolic nature of the transport equation of the conformation tensor, Eq. (2.3), caused by the absence of diffusion (Dubief *et al.* 2005). For $Re < Re_c$, a perfectly laminar flow stretches polymers through the action of shear (stretching term in Eq. 2.3). The introduction of small perturbations into the flow excites the unstable nature of the nonlinear advection term $(\mathbf{u}\cdot\boldsymbol{\nabla})\mathbf{C}$, resulting in the formation of sheets or cliffs of polymer stretch akin to cliffs of scalar concentration observed in the turbulent transport of low-diffusivity passive scalar (Schumacher *et al.* 2005). This behavior is obvious when comparing Figure 2(b-c) with LIF (Laser Induced Fluorescein) images of fluorescein dye concentration in polymer drag-reduced wall bounded flows (Somandepalli *et al.* 2010). The sheets of high polymer stretch, hosting a significant increase in extensional viscosity, create a strong local anisotropy, with a formation of local low-speed jet-like flow. The response of the flow is through pressure (Eq. 4.1), whose role is to redistribute energy across components of momentum, resulting in the formation of waves, or trains of alternating rotational and straining motions as shown by the Q_a isosurfaces. The mechanism shares some similarity with the Kelvin-Helmholtz instability, except that the thickness of these sheets is too close to the Kolmogorov scale (smallest scale of turbulence) for vortices to be created. Once triggered, EIT is self-sustained since the elastic instability creates the very velocity fluctuations it feeds upon. Interestingly, Samanta *et al.* (2012) and Dubief *et al.* (2010) show that the phenomenon of EIT is not confined to low Reynolds numbers, unlike elastic turbulence (Groisman & Steinberg 2000).

5. The onset of EIT in bypass transition

To highlight the sensitivity of polymer flows to perturbations and the relevance of Eq. (4.1), we analyzed a bypass transition initiated during the 2010 Summer Program. The setup is described in Dubief *et al.* (2010) and summarized here. A periodic channel flow at $Re = 10000$ is initialized with a uniform mean velocity flow. The channel core (half the channel thickness) contains isotropic turbulence at a prescribed turbulence intensity level. In a region of one quarter of channel height thick adjacent to the wall, the flow is totally free of turbulence, thus allowing the development of laminar boundary layers on both walls. The relevance of this simulation within the present discussion is the observation that (i) the onset of turbulence in the presence of polymers happens well before the core turbulence diffuses into the near-wall region and (ii) turbulence (EIT) occurs for an initial turbulent intensity of the initial perturbation well below the minimal level required to trigger turbulence in a Newtonian flow (Dubief *et al.* 2010).

During the early stage of the transition, the rapid growth of EIT with the absence of direct velocity perturbations (the diffusion of the core turbulence is slow) is indicative of a

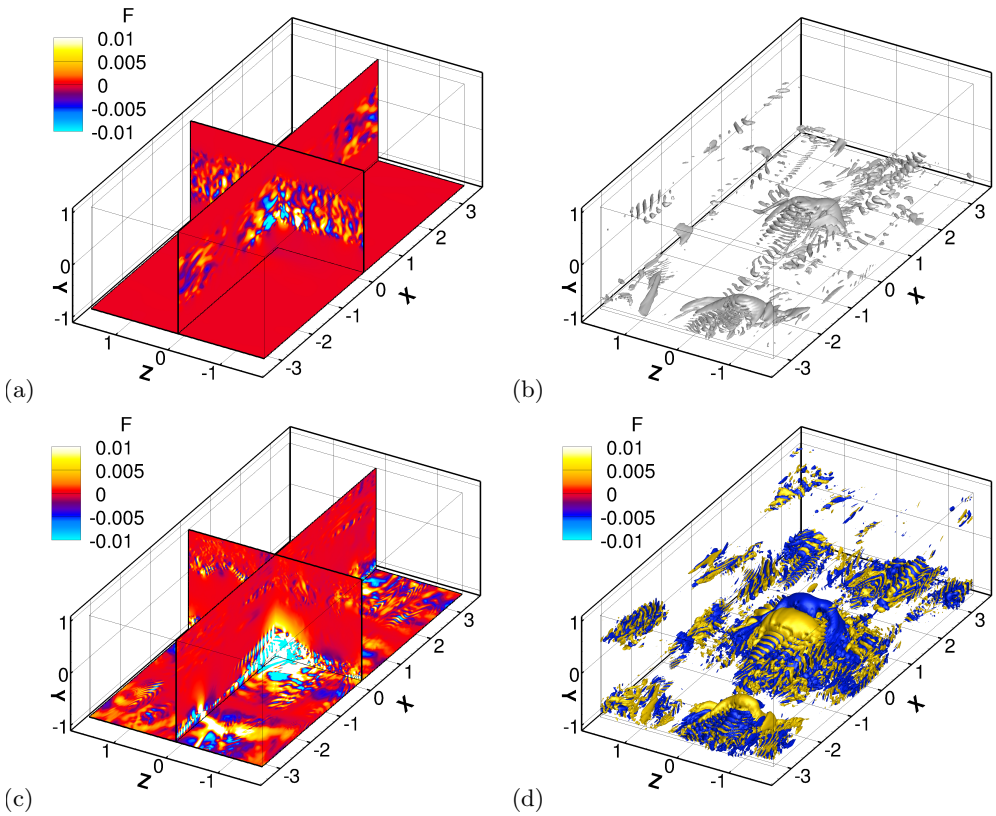

FIGURE 3. Distribution of the integrant F in Eq. (5.3) for the calculation of pressure (Eq. 5.2) at location $\boldsymbol{\xi} = (0, -0.9h, 0)$ in a bypass transition channel flow at $Re = 10000$ (Dubief *et al.* 2010). (a) Shows the distribution of F at an early stage of the transition when the flow close to the wall is essentially laminar. Near-wall pressure perturbations are shown to be triggered by the core flow through a receptivity mechanism. (b) Visualization of positive Q_a structures highlighting the existence of hairpin-like vortices as well as small-scale elastic instabilities in the fully developed stage of MDR at $Re = 10000$. For the same location $\boldsymbol{\xi}$ as in (a), (c) and (d) show the distribution of F corresponding to the flow field (b), in planes and 3D isosurfaces, respectively. Notice that the F values generated by small-scale elastic instabilities are of the same order of magnitude as the contribution of large-scale vortices. (Color online.)

receptivity mechanism through pressure. To illustrate this mechanism, we investigate the spatial distribution of the integrant, or influence function, F in the solution of Eq. (4.1)

$$p(\boldsymbol{\xi}) = \int_V G(\boldsymbol{\xi}, \mathbf{x}) f(\mathbf{x}) \mathrm{d}\mathbf{x} \equiv \int_V F(\boldsymbol{\xi}, \mathbf{x}) \mathrm{d}\mathbf{x} \tag{5.1}$$

at a location close to the bottom wall, $\boldsymbol{\xi} = (0, -0.9h, 0)$, where h is the half-height of the domain and coordinates are defined in Figure 3. The influence function $F(\boldsymbol{\xi}, \mathbf{x}) = G(\boldsymbol{\xi}, \mathbf{x}) f(\mathbf{x})$ represents the contribution of any point $\mathbf{x}$ to the pressure at location $\boldsymbol{\xi}$.

Green's function G in an infinite domain is simply the harmonic function $|\boldsymbol{\xi} - \mathbf{x}|^{-1}$. However, in the case of a channel flow, the domain is finite and the periodic and wall boundary conditions must be considered. Following Mansour *et al.* (1988) and Kim (1989), we assume that the normal pressure derivative vanishes at the walls. Using a spectral

transformation in the periodic directions x and z, it can be shown that the pressure at $\boldsymbol{\xi}$ can be written as

$$p(\xi,\eta,\zeta) = \int_0^{L_x}\int_{-H/2}^{H/2}\int_0^{L_z} F(\xi,\eta,\zeta,x,y,z)\mathrm{d}x\mathrm{d}y\mathrm{d}z. \tag{5.2}$$

We are interested in the function F, which is

$$F(\xi,\eta,\zeta,x,y,z) = \frac{1}{L_xL_z}G(\xi-x,\eta,\zeta-z,y)f(x,y,z), \tag{5.3}$$

where $G(\xi,\eta,\zeta,y) = \mathcal{F}^{-1}(\hat{G}(k_x,\eta,k_z,y))$. In other words, Green's function G is obtained from its Fourier coefficients $\hat{G}$ that are defined as

$$\hat{G}(k_x,\eta,k_z,y) = \begin{cases} -\frac{\cosh(k'(\eta+y))+\cosh(k'H-k'|y-\eta|)}{2k'\sinh(k'H)}, & k'\neq 0, \\ -\frac{y^2}{2H} - \frac{1}{2}y + \max(\eta,y), & k'=0, \end{cases} \tag{5.4}$$

with $k'^2 = (k'^2_x + k'^2_y)$, $k'_x = 2\pi k_x/L_x$ and $k'_z = 2\pi k_z/L_z$.

Figure 3(a) shows that the main contribution to near-wall pressure is the core turbulence. EIT is therefore triggered by pressure fluctuations created by long-range interactions, not short-range velocity perturbations arising from the wall as in Eq. (2.4). The rapid growth of EIT observed by Dubief *et al.* (2010) in this flow suggests that the pressure driven pertubation excites the most unstable term in the transport equation of the conformation tensor Eq. (2.3), which is the advection term due to the absence of diffusion of $\mathbf{C}$, thus highlighting the inertial component of EIT.

Although the Reynolds number is not large by separation of scales' standard, it is large enough to study the influence of elastic instabilities in the fully developed MDR flow subsequent to the onset of EIT shown in Figures 3(b-d). Figure 3(b) depicts an active state of MDR (Xi & Graham 2010) where hairpin-like vortices are identified using positive-Q_a isosurfaces. The large scales educed by the positive isosurfaces are vortices. Note the trains of small-scale structures in the wake of the head of vortices capturing the extensional flow elastic instability. Figures 3(c-d) show the distribution of the influence function F represented in planes (c) and isosurfaces (d) for the same $\boldsymbol{\xi}$ as in (a), which happens to sit below a large hairpin vortex. The influence of the vortex is prominent; however, the small-scale elastic instabilities are all captured throughout the domain, providing a clear evidence of the influence of small-scale polymer dynamics on the flow.

6. Conclusion

Elasto-inertial turbulence offers a new perspective on polymer drag reduction. First, it provides support to De Gennes (1990)'s theory of energy transfers between polymers and flow. Second, EIT allows us to consider the possible structure of MDR for very large elasticity ($Wi \to \infty$): The sheer magnitude of extensional viscosity is likely to prevent the emergence of any vortical structures, thus leaving MDR to be sustained by near-wall spanwise structures similar to the ones observed at low Reynolds numbers (Figure 2d).

The asymptotic state of polymer drag reduction in the absence, or near absence, of vortices should therefore to be driven by the nonlinear transport of polymer stretch, which resembles the transport of a high Schmidt number passive scalar, and the response of the flow to a sheet-like, strongly anisotropic field of effective viscosity governed by the extensional viscosity of polymers. As discussed by Dubief *et al.* (2010) and Dubief *et al.* (2012), the flow is therefore stuck in a transitional state, specifically the stage

of breakdown of nonlinear flow instabilities, which does not support a logarithmic mean velocity profile (Klewicki *et al.* 2011). Unfortunately, a major obstacle in the derivation of a low Reynolds (or possibly high Reynolds) number correction of Virk's log law is the lack of theoretical understanding of high Schmidt number active scalar transport in nonlinear anisotropic flows. A spectral analysis of the turbulent kinetic energy and polymer stress of EIT (not shown) indicates strong similarities with passive scalar transport, in particular with the existence of a viscous-convective range at small scales (Batchelor *et al.* 1959). Yet the spectral decay in polymer elastic energy and polymer stretch appears to be steeper than k^{-1}. Future research should therefore focus on the dynamics of active scalars and the backscatter of energy caused by small-scale polymer dynamics. Another interesting future research direction was brought to our attention by our reviewer Dr. Olaf Marxen who questioned whether the action of the polymers in the flow is catalytic or one of direct energy exchange between polymer and flow instabilities. At low Reynolds numbers, the process appears to be a direct energy exchange; however, certain aspects of EIT at high Reynolds numbers may be catalytic, e.g. the trigger of elastic instability through bypass transition.

EIT has much broader impacts than polymer drag reduction. In addition to active scalar transport, we believe EIT could be found in other viscoelastic fluids, provided that these fluids possess a similar rheological response in extensional flows and low diffusivity.

Acknowledgments

The Vermont Advanced Computing Center is gratefully acknowledged for providing the computing resources necessary for our simulations. YD acknowledges the support of grant No. P01HL46703 (project 1) from the National Institutes of Health. VET acknowledges the financial support of a Marie Curie FP7 Career Integration Grant within the 7th European Community Framework Programme (Grant Agreement n° PCIG10-GA-2011-304073). JS acknowledges the support of the Australian Research Council.

REFERENCES

Batchelor, G. K., Howells, I. D. & Townsend, A. A. 1959 Small-scale variation of convected quantities like temperature in turbulent fluid. Part 2: The case of large conductivity. *J. Fluid Mech.* **5** (01), 134–139.

Bird, R., Armstrong, R. & Hassager, O. 1987 *Dynamics of Polymeric Liquids. Vol. 2: Kinetic Theory*. Wiley-Interscience, 1987,.

De Gennes, P. 1990 *Introduction to Polymer Dynamics*. Cambridge Univ Pr.

Dubief, Y., Terrapon, V., White, C., Shaqfeh, E., Moin, P. & Lele, S. 2005 New answers on the interaction between polymers and vortices in turbulent flows. *Flow, Turbulence and Combustion* **74** (4), 311–329.

Dubief, Y., White, C., Terrapon, V., Shaqfeh, E., Moin, P. & Lele, S. 2004 On the coherent drag-reducing and turbulence-enhancing behaviour of polymers in wall flows. *J. Fluid Mech.* **514**, 271–280.

Dubief, Y., White, C. M., Shaqfeh, E. S. G. & Terrapon, V. E. 2010 Polymer maximum drag reduction: A unique transitional state. In *Annual Research Briefs*, pp. 395–404. Center for Turbulence Research, Stanford, CA.

Dubief, Y., White, C. M., Shaqfeh, E. S. G. & Terrapon, V. E. 2012 Polymer maximum drag reduction: A unique transitional state. *Phys. Fluids* Submitted.

Groisman, A. & Steinberg, V. 2000 Elastic turbulence in a polymer solution flow. *Nature* **405** (6782), 53–55.

Hoyt, J. 1977 Laminar-turbulent transition in polymer solutions. *Nature* **270**, 508–509.

Kim, J. 1989 On the structure of pressure fluctuations in simulated turbulent channel flow. *J. Fluid Mech.* **205**, 421–451.

Kim, K., Li, C., Sureshkumar, R., Balachandar, S. & Adrian, R. 2007 Effects of polymer stresses on eddy structures in drag-reduced turbulent channel flow. *J. Fluid Mech.* **584**, 281–299.

Klewicki, J., Ebner, R. & Wu, X. 2011 Mean dynamics of transitional boundary-layer flow. *J. Fluid Mech.* **682**, 617–651.

Li, C., Sureshkumar, R. & Khomami, B. 2006 Influence of rheological parameters on polymer induced turbulent drag reduction. *J. non-Newtonian Fluid Mech.* **140** (1-3), 23–40.

Mansour, N. N., Kim, J. & Moin, P. 1988 Reynolds-stress and dissipation-rate budgets in a turbulent channel flow. *J. Fluid Mech.* **194** (1), 15–44.

Ooi, A., Martin, J., Soria, J. & Chong, M. 1999 A study of the evolution and characteristics of the invariants of the velocity-gradient tensor in isotropic turbulence. *J. Fluid Mech.* **381**, 141–174.

Procaccia, I., Lvov, V. & Benzi, R. 2008 Colloquium: Theory of drag reduction by polymers in wall-bounded turbulence. *Rev. Modern Phys.* **80** (1), 225.

Samanta, D., Dubief, Y., Holzner, M., Schäfer, C., Morozov, A., Wagner, C. & Hof, B. 2012 Elasto-inertial turbulence. *Submitted* .

Schumacher, J., Sreenivasan, K. & Yeung, P. 2005 Very fine structures in scalar mixing. *J. Fluid Mech.* **531**, 113–122.

Somandepalli, V., Hou, Y. & Mungal, M. 2010 Concentration flux measurements in a polymer drag-reduced turbulent boundary layer. *J. Fluid Mech.* **644**, 281–319.

Soria, J., Sondergaard, R., Cantwell, B., Chong, M. & Perry, A. 1994 A study of the fine-scale motions of incompressible time-developing mixing layers. *Phys. Fluids* **6** (2), 871–884.

Terrapon, V., Dubief, Y., Moin, P., Shaqfeh, E. & Lele, S. 2004 Simulated polymer stretch in a turbulent flow using Brownian dynamics. *J. Fluid Mech.* **504**, 61–71.

Virk, P., Mickley, H. & Smith, K. 1970 The ultimate asymptote and mean flow structure in Toms phenomenon. *Trans. ASME E: J. Appl. Mech* **37**, 488–493.

White, C., Dubief, Y. & Klewicki, J. 2012 Re-examining the logarithmic dependence of the mean velocity distribution in polymer drag reduced wall-bounded flow. *Phys. Fluids* **24** (2), 021701–021701.

White, C. & Mungal, M. 2008 Mechanics and prediction of turbulent drag reduction with polymer additives. *Annu. Rev. Fluid Mech.* **40** (1), 235–256.

Xi, L. & Graham, M. 2010 Active and hibernating turbulence in minimal channel flow of Newtonian and polymeric fluids. *Phys. Rev. Lett.* **104** (21), 218301.